Interactions in 2D electron and hole systems in the intermediate and ballistic regimes

2003 J. Phys. A: Math. Gen. 36 9249

(http://iopscience.iop.org/0305-4470/36/35/311)

INSTITUTE OF PHYSICS PUBLISHING JOURNAL OF PHYSICS A: MATHEMATICAL AND GENERAL

J. Phys. A: Math. Gen. **36** (2003) 9249–9262 PII: S0305-4470(03)60888-7

Interactions in 2D electron and hole systems in the intermediate and ballistic regimes

Y Y Proskuryakov[1], A K Savchenko[1], S S Safonov[1], L Li[1], M Pepper[2], M Y Simmons[2], D A Ritchie[2], E H Linfield[2] and Z D Kvon[3]

[1] School of Physics, University of Exeter, Stocker Road, Exeter, EX4 4QL, UK
[2] Cavendish Laboratory, University of Cambridge, Madingley Road, Cambridge CB3 0HE, UK
[3] Institute of Semiconductor Physics, Novosibirsk, 630090, Russia

Received 14 March 2003, in final form 24 June 2003
Published 20 August 2003
Online at stacks.iop.org/JPhysA/36/9249

Abstract

In different 2D semiconductor systems we study the interaction correction to the Drude conductivity in the intermediate and ballistic regimes, where the parameter $k_B T\tau/\hbar$ changes from 0.1 to 10 (τ is momentum relaxation time). The temperature dependence of the resistance and magnetoresistance in parallel and perpendicular magnetic fields is analysed in terms of the recent theories of electron–electron interactions in systems with different degree of disorder and different character of the fluctuation potential. Generally, good agreement is found between the experiments and the theories.

PACS numbers: 71.30.+h, 73.40.Qv

1. Introduction

The problem of the origin of the metallic behaviour of high-mobility 2D electron and hole gases (2DEG, 2DHG) has been intensively studied in the last few years [1]. In these systems the resistance shows an increase with increasing temperature which is in contradiction with the scaling theory of localization. As the localization theory does not take into account electron–electron interactions, their role has to be questioned, especially because the ratio r_s of the Coulomb energy to the Fermi energy is large in these low-density systems ($r_s \sim 10$).

The well-established theory [2, 3] of the interaction correction to the Drude conductivity σ_0 has considered the 'diffusive' regime, $k_B T\tau/\hbar < 1$, which is not applicable for high-mobility carriers. Recently, a theory of the interaction correction in the ballistic ($k_B T\tau/\hbar > 1$) and intermediate regimes has been developed [4]. This theory considers electron interaction mediated by only a few impurities. It involves coherent electron backscattering from an impurity and from the modulated density of other electrons (Friedel oscillations) caused by this impurity with a short-range potential.

This condition of point-like scatterers is satisfied in Si MOSFET structures [5] and very high-mobility GaAs structures with a large spacer ($d \sim 500$–1000 Å) [6, 7] where

carrier scattering is dominated by background impurities in the 2D channel. To examine the predictions of the theory [4] we study both these systems: vicinal Si MOSFETs and p-GaAs heterostructures with $d = 500$ Å .

Short-range scatterers, however, are not common in GaAs heterostructures where doping impurities are separated from the 2D channel by a thinner spacer ($d < 300$ Å). In this case the scattering potential has a long-range character [7, 8], with the correlation length equal to the spacer thickness. Then the correction in [4] is expected to be negligible, because in the presence of the long-range potential both the Friedel oscillation and the backscattering are weak. However, it was shown in the latest theory [9] that applying a strong magnetic field increases the probability of an electron returning back and thus restores the interaction correction. To test this prediction we study a high-mobility 2DEG in an n-GaAs heterostructure with $d = 200$ Å .

Our investigations of interaction effects in the three types of 2D structure cover the range $k_B T\tau/\hbar \sim (0.1\text{–}10)$ and show good agreement with the recent theories.

2. Predictions of the new interaction theories

For the ballistic regime the interaction theory [4] gives several predictions. *Firstly*, the correction has a linear temperature dependence at $k_B T\tau/\hbar > 1$:

$$\delta\sigma_{xx}(T) = \sigma_0 \left(1 + \frac{3F_0^\sigma}{1 + F_0^\sigma}\right) \frac{k_B T}{E_F} \tag{1}$$

where F_0^σ is the Fermi liquid interaction parameter in the triplet channel. The coefficient in the temperature dependence originates from two contributions: the first is due to exchange processes (Fock) and the second is due to direct interaction (Hartree). *Secondly*, for a wide range of parameter F_0^σ the model allows the change in the sign of $\mathrm{d}\rho/\mathrm{d}T$ with parallel magnetic field from positive to negative, the effect seen in recent experiments [1]. (Negative $\mathrm{d}\sigma_{xx}/\mathrm{d}T$ corresponds to large enough negative F_0^σ.) A magnetic field suppresses the triplet channel term in equation (1), resulting in a universal, positive correction to the Drude conductivity in magnetic field, σ_0^B, and hence the insulating $\rho(T)$:

$$\delta\sigma = \sigma_0^B \frac{T}{T_F} \qquad \text{at} \quad B \geqslant B_S. \tag{2}$$

Here B_S is the field corresponding to the full spin polarization of the 2D system, $B_S = 2E_F/g^*\mu_B$, where g^* is the Lande g-factor, μ_B is the Bohr magneton and T_F is the Fermi temperature.

In the case of a long-range scattering potential, the theory [9] shows that a classically strong magnetic field, $\omega_c\tau > 1$, perpendicular to the 2D plane restores the correction $\delta\sigma_{xx}(T)$, which can be detected by the parabolic negative magnetoresistance:

$$\rho_{xx} = \frac{1}{\sigma_0} + \frac{1}{\sigma_0^2}(\mu^2 B^2)\delta\sigma_{xx}(T). \tag{3}$$

In the diffusive regime, where strong magnetic fields do not affect the correction, $\delta\sigma_{xx}(T)$ is described by the theory [2], provided the effect of Zeeman splitting on interactions is negligible. In the ballistic regime, however, $\delta\sigma_{xx}(T)$ found from the negative magnetoresistance in equation (3) will be significantly weaker than that in equation (1) which is valid for a short-range potential.

3. Results on p-GaAs

3.1. Samples

The first set of experiments has been performed on a 2DHG in a (311)*A* modulation doped GaAs/AlGaAs heterostructure with a spacer $d = 500$ Å and peak mobility of 6.5×10^5 cm^2 V^{-1} s^{-1}. This system shows the crossover from metal to insulator at $p \sim 1.5 \times 10^{10}$ cm^{-2} [10]. The hole density p in the metallic region is varied in the range $(2.09–9.4) \times 10^{10}$ cm^{-2} ($r_s = 10–17$).

3.2. Effective mass of holes at low densities

In the analysis of the transport properties of low-density 2D systems, it is important to know the density dependence of the carrier effective mass m^* [11–13]. In the case of a 2DHG in GaAs the value of m^* is not well known at $p < 10^{11}$ cm^{-2}. Therefore, we have especially performed an analysis of the temperature dependence of Shubnikov–de Haas (SdH) oscillations measured in weak magnetic fields and extracted the value of the effective mass at different hole densities from 2.9×10^{10} to 8.2×10^{10} cm^{-2} (close to the borders of the studied range of p).

A typical trace of the oscillating component of ρ_{xx} obtained after the subtraction of the monotonic background is shown in the inset to figure 1(*a*) by symbols, together with the fit (solid line) to the conventional theoretical expression for the SdH effect [14, 15]:

$$\frac{\delta\rho_{xx}}{\rho_0} = \sum_s 4\exp\left(-\frac{2\pi^2 s}{\mu_q B}\right)\frac{2\pi^2 s k_B T/\hbar\omega_c}{\sinh(2\pi^2 s k_B T/\hbar\omega_c)}\cos\left[\frac{\hbar\pi^2 s n}{eB_\perp} - \pi s\right]. \quad (4)$$

Here $\rho_0 = \rho_{xx}(B = 0)$, $\omega_c = eB/m^*$ is the cyclotron frequency, μ_q is the quantum mobility proportional to the quantum lifetime $\tau_q = m^*\mu_q/e$. As seen from the plot, the experimental oscillations are well described by the theoretical dependence (4) where we use only the first harmonic, $s = 1$. The fit is made using m^* and μ_q as free parameters. (Here and in other figures the indicated hole density p is determined from the period of SdH oscillations.)

In figure 1(*a*) the amplitudes of low-field oscillations $\Delta\rho^A_{xx}$, taken both in minima and maxima, are shown for different temperatures by solid symbols. We have found that all our data $\Delta\rho^A_{xx}(B^{-1})$ are fitted best when m^* is close to $0.38m_e$ and μ_q is allowed to be T-dependent (figures 1(*a*) and (*b*)). Taking different values of m^* for all p gave either a worse fit or unreasonably large μ_q (see dashed lines in figure 1).

It has been found that the temperature dependence of μ_q becomes weaker at lower densities, close to the metal-to-insulator crossover. Thus we have found that SdH oscillations at a low density $p = 2.9 \times 10^{10}$ cm^{-2} can be well described by the conventional approach: assuming that μ_q is T-independent (see the Dingle plot in the inset to figure 1(*b*), where m^* is used as the only free parameter). The value $m^* = 0.38m_e$ obtained here is in excellent agreement with the mass obtained at higher studied densities and with the value $m^* = (0.37–0.38)m_e$ previously reported for hole densities above 7×10^{10} cm^{-2} [16]. This shows that the effective mass of the 2DHG in the low-density p-GaAs heterostructure, $m^* = (0.38 \pm 0.02)m_e$, is essentially independent of the hole density within the experimental accuracy. (Recent investigation of the 2DEG in n-GaAs heterostructures [17] has also shown independence of the effective mass of electrons down to densities as low as $(1.4–3) \times 10^{10}$ cm^{-2}.)

3.3. Temperature dependence of resistivity and metallic behaviour

Figure 2(*a*) represents the temperature dependence of the resistivity, with the dashed box indicating the curves we analysed. The increase of the resistivity with T can be simply due to

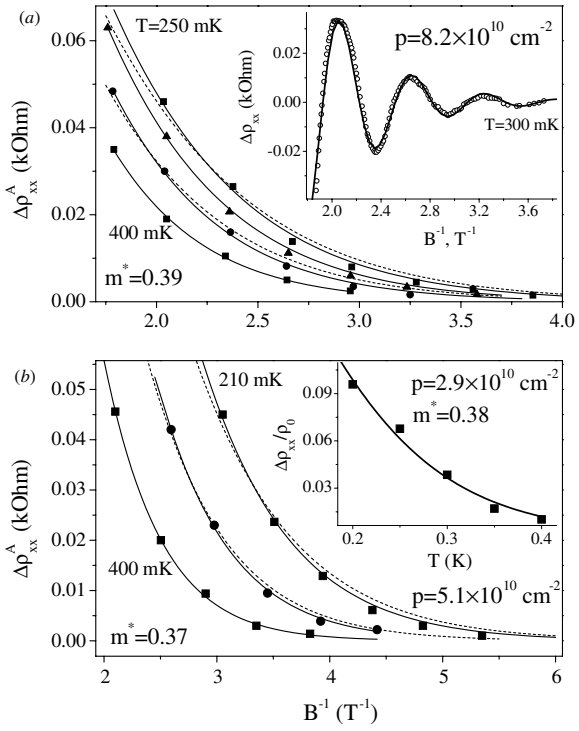

Figure 1. Inset to (*a*): a typical trace of the SdH oscillations in $\rho_{xx}(B^{-1})$ after subtraction of the monotonic background (solid line is the fit to equation (4)). Fitting parameters of the solid line are: $m^* = (0.39 \pm 0.01)m_e$ and $\mu_q = 6.5 \times 10^4$ cm^2 V^{-1} s^{-1}. (*a*) Amplitudes of oscillations $\triangle\rho^A_{xx}$ at $T = 250, 300, 350$ and 450 mK, for $p = 8.2 \times 10^{10}$ cm^{-2}. Solid lines are the fit to equation (4) with $m^* = (0.39 \pm 0.01)m_e$ and $\mu_q = (5.4, 6.5, 7.3, 7.8 \pm 0.2) \times 10^4$ cm^2 V^{-1} s^{-1} for these T, respectively. (*b*) Similar results for $p = 5.1 \times 10^{10}$ cm^{-2}. The best fit (solid lines) achieved with $m^* = (0.37 \pm 0.01)m_e$ and $\mu_q = (7.13, 7.4, 7.85 \pm 0.15) \times 10^4$ cm^2 V^{-1} s^{-1} for $T = 210$, 300, 400 mK, respectively. Dashed lines in (*a*) and (*b*) are fits to equation (4) with slightly different masses ($m^* = 0.33m_e$ in (*a*), and $m^* = 0.31m_e$ in (*b*); μ_q used as a free parameter). Inset to (*b*): the amplitude $\triangle\rho^A_{xx}$ at a low density, $p = 2.9 \times 10^{10}$ cm^{-2}, at $B = 0.4$ T and different temperatures. Solid line is a one-parameter fit to the temperature-dependent factor in equation (4) with $m^* = 0.38m_e$ (μ_q is eliminated in this approach).

phonon scattering, which cannot be ignored even at temperatures below 1 K in GaAs structures where piezoelectric coupling is important. In figures 2(*b*)–(g), the curves $\rho(T)$ for different densities are plotted together with the theoretical dependence presented as $\rho(T) = \rho_0 + \rho_{\rm ph}$, where $\rho_0 = \rho(T = 0) = \sigma_0^{-1}$ is the residual resistivity due to impurity scattering, obtained by extrapolation of experimental curves to $T = 0$, and $\rho_{\rm ph}$ is the result of calculations for phonon scattering in GaAs heterostructures [18]. The latter is represented as $\rho_{\rm ph}(T) = \frac{a(T/T_0)^3}{1+c(T/T_0)^2}$, where parameters a and c depend on the carrier density, effective mass and crystal properties, and $T_0 = k_B^{-1}\sqrt{2m^* S_t^2 E_F}$, where S_t is the transverse sound velocity.

One can see in figure 2(*a*) that at the highest p, phonon scattering (bold curve) is strong enough to explain the experimental dependence $\rho(T)$. However, with decreasing density another contribution develops, figures 2(*b*)–(*g*), which totally dominates at low T and low densities. Figure 3(*a*) shows this contribution obtained by subtracting the contribution to the resistivity of phonon scattering. The peak in $\rho(T)$, with a maximum at $T_{\rm max} \approx 0.3T_F$, is in

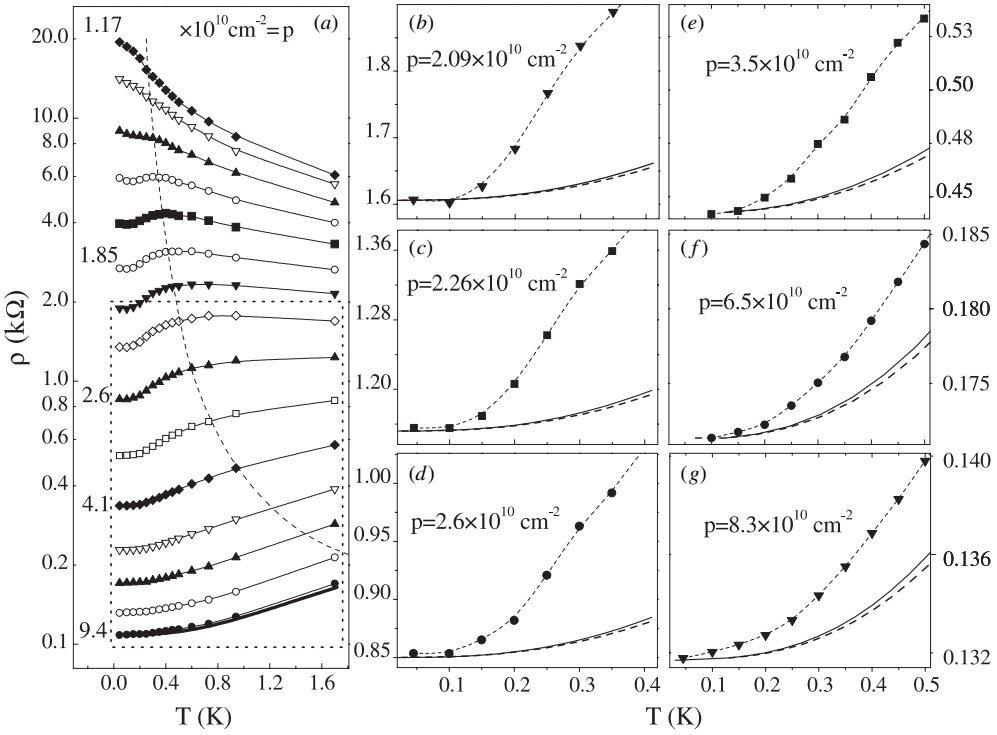

Figure 2. (*a*) Temperature dependence of the resistivity at different hole densities near the crossover in the sign of $\mathrm{d}\rho/\mathrm{d}T$. The bold line at the bottom of the plot ($p = 9.4 \times 10^{10}$ cm^{-2}) is the calculated $\rho(T)$ due to phonon scattering. (*b*)–(*g*) Resistivity on the metallic side of the crossover (symbols), together with the calculated contribution to $\rho(T)$ due to phonon scattering (solid lines: with $m^* = 0.38m_e$; dashed lines: with $m^* = 0.36m_e$).

qualitative agreement with the expectation that after the transition to the nondegenerate state the resistance should decrease with increasing temperature [19, 20].

In order to compare the results in the low-temperature range of $\rho(T)$ with equation (1), we replot the data in figure 3(*b*) in the conductivity form: $\Delta\sigma(T) = (\rho(T) - \rho_{\mathrm{ph}}(T))^{-1} - \rho_0^{-1}$. The condition for the ballistic regime $k_B T\tau/\hbar \geqslant 1$ is satisfied in our structure at $T > 50$–100 mK, and a linear fit of $\Delta\sigma(T)$ gives the value of the parameter F_0^σ, figure 3(*c*). (It should be noted that the accuracy in determining m^* (section 3.2) does not affect our results—see dashed lines in figures 2(*b*)–(*g*) for a different value of m^*.)

3.4. Short-range scattering potential

To establish the character of the fluctuation potential in our structure we calculate the expected momentum relaxation rate $\tau^{-1}(T = 0)$ at different hole densities for both homogeneous background and remote doping. To do this we use the experimental parameters of the studied structure (the spacer thickness and doping concentration) and the expressions in [7, 21] for τ^{-1} in terms of these parameters. In figure 4 we plot the result of calculations together with the experimental values obtained from the Drude resistivity ($\rho_0 = m^*/e^2\tau p$) in the metallic regime ($p \geqslant 2 \times 10^{10}$ cm^{-2}). As seen in the plot, the values of $\tau^{-1}(p, T = 0)$ calculated for remote acceptor scattering (dashed line) are an order of magnitude smaller than the experimental ones.

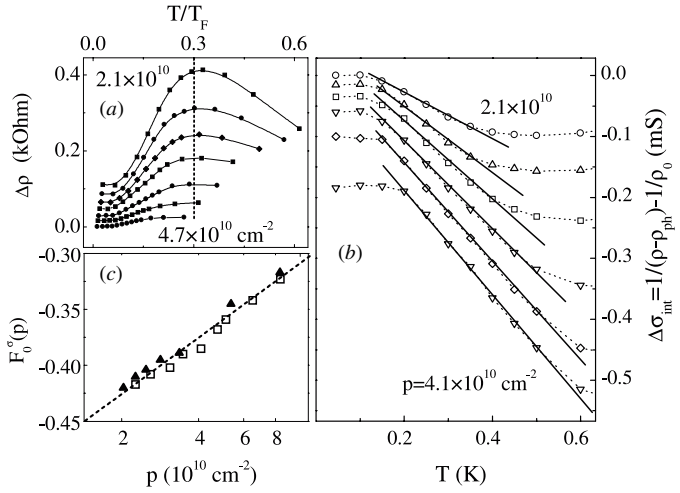

Figure 3. (*a*) Impurity scattering contribution $\Delta\rho$ against dimensionless temperature at different p. (For clarity, curves in (*a*) and (*b*) are offset vertically from the zero value at $T = 0$.) (*b*) The same data as in (*a*) but in the conductivity form, with linear fitting. (*c*) Fermi liquid parameter versus hole density. Open symbols show the result obtained from the analysis of $\rho(T)$ at zero magnetic field; closed symbols show the result from the analysis of the parallel-field magnetoresistance, figure 6(*d*).

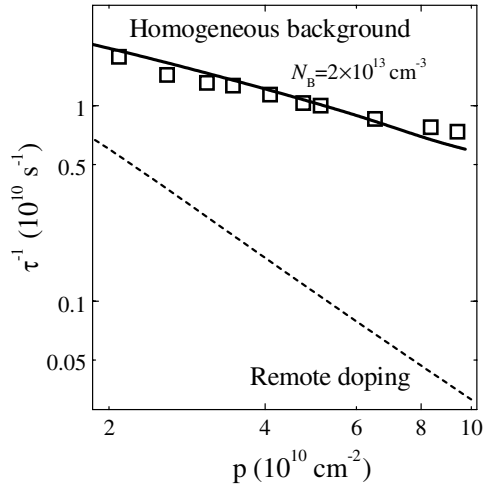

Figure 4. Density dependence of the momentum relaxation rate. Symbols: experiment; solid line: calculation for homogeneous background doping; and dashed line: calculation for remote doping.

The calculated result for homogeneous background doping is depicted by the solid line. To plot it we use the density of the background impurities N_B as the only adjustable parameter and find reasonable agreement with experiment. The obtained value $N_B = 2 \times 10^{13}$ cm^{-3} is close to the value expected for the wafer growth conditions: (3–5) $\times 10^{13}$ cm^{-3}. This is also close to typical values for n-type heterostructures with $\mu \sim 3 \times 10^5$–10^7 cm^2 V^{-1} s^{-1} and a comparable spacer width 300–700 Å : $N_B \sim 10^{13}$–10^{14} cm^{-3} [6, 7]. Thus, one can conclude that the dominating scattering in our system is due to background impurities with a

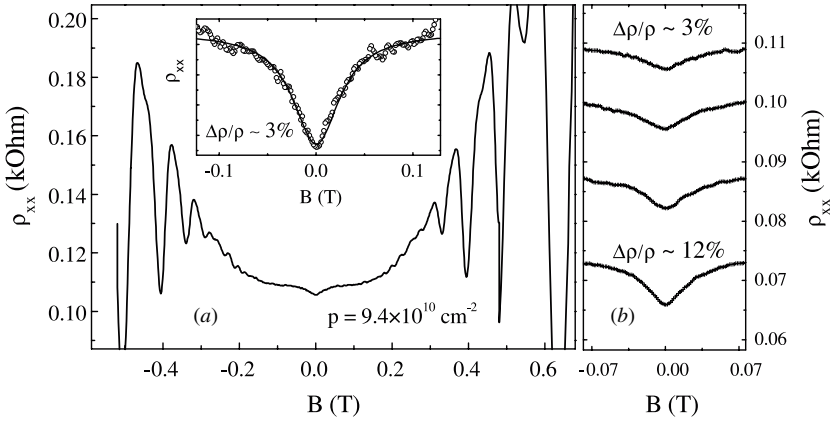

Figure 5. (*a*) Perpendicular-field magnetoresistance $\rho_{xx}(B)$ at $p = 9.4 \times 10^{10}$ cm^{-2}, $T = 45$ mK. Inset: zoomed-in low-field region; the solid line is the fit to equation (5). (*b*) $\rho_{xx}(B)$ at different hole densities: from 9.4×10^{10} (top) to 1.7×10^{11} cm^{-2} (bottom). Numbers indicate the magnitude of magnetoresistance in percentage of the zero-field resistivity.

short-range random potential. This means that the approximation of the theory [4] can indeed be applied and our analysis in [22] is justified.

3.5. The effect of split bands on the metallic behaviour

According to [23, 24], $\mathrm{d}\rho/\mathrm{d}T > 0$ in a high-density 2DHG in GaAs structures can, in principle, be explained in terms of inelastic scattering between two subbands which are split due to strong spin–orbit interactions. The metallic behaviour is then accompanied by positive magnetoresistance (PMR) in a magnetic field perpendicular to the plane. According to the experimental and theoretical studies [24] this PMR is described by

$$\rho_{xx}(B) = \rho_{xx}(B \to \infty) + \frac{L}{1 + (B/W)^2} \tag{5}$$

where

$$\rho_{xx}(B \to \infty) = \frac{R_1^2 S_2 + R_2^2 S_1 - 2QR_1R_2}{(R_1 + R_2)^2} \qquad W = \frac{S_1 + S_2 + 2Q}{R_1 + R_2}$$
$$L = -\frac{[R_2(S_1 + Q) - R_1(S_2 + Q)]^2}{(S_1 + S_2 + 2Q)(R_1 + R_2)^2}.$$

Here $R_i = 1/ep_i$ is the Hall coefficient of the ith subband. The elements S_1, S_2 and Q are scattering rates, which are determined by intra- and interband scattering mechanisms (both elastic and inelastic).

Now we investigate the relevance of this mechanism to our system. In figure 5(*a*) the trace $\rho_{xx}(B)$ is shown for the highest studied hole density $p = 9.4 \times 10^{10}$ cm^{-2}, section 3.3, where a weak PMR of a similar shape to that in [24] is observed. In the inset a zoom-in of the lower field data is plotted as well as its fit to equation (5) using scattering rates as adjustable parameters. It is seen that the theory describes well the experiment. The scattering rates obtained are of the same order of magnitude as those in [24].

According to [24], the magnitude of PMR at $T = 0$ and the magnitude of the drop in $\rho(T)$ from $T \sim 100$ K to $T = 0$ are determined by the same interband inelastic scattering

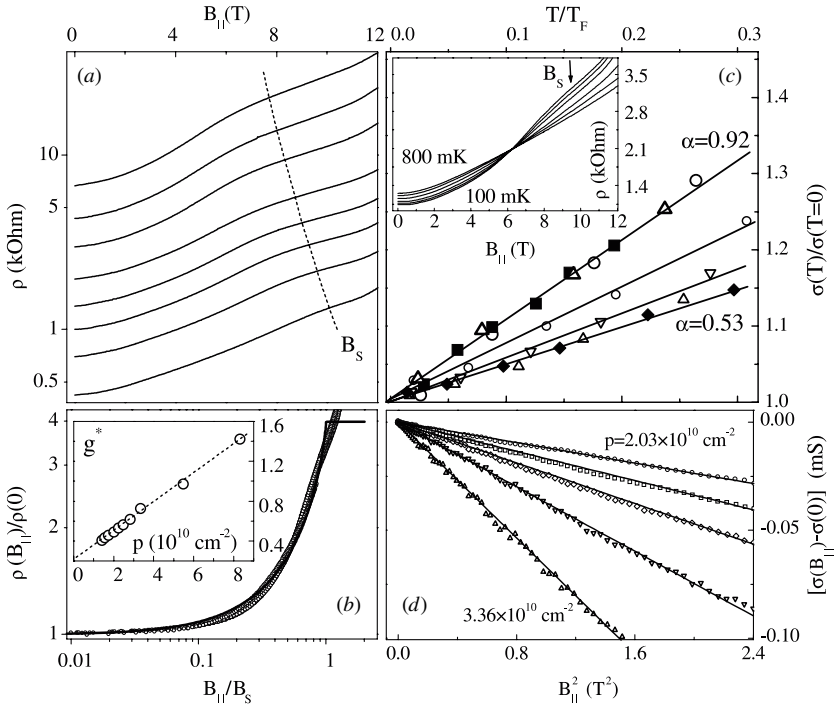

Figure 6. (*a*) Dependence of the resistivity on parallel magnetic field at $T = 50$ mK and $p = (1.43, 1.57, 1.75, 2.03, 2.26, 2.49, 2.83, 3.36) \times 10^{10}$ cm^{-2}, from top to bottom. (*b*) Scaled data, with an added curve $\rho(B_\parallel)$ for $p = 8.34 \times 10^{10}$ cm^{-2}; solid line is the result of the model 27. Inset: dependence of the effective g-factor on the hole density, obtained from the value of B_S. (*c*) Temperature dependence of the conductivity at $B_\parallel = B_S$ for different hole densities. Coefficient $\alpha = 0.53$ is obtained for $p = (2.49, 2.83) \times 10^{10}$ cm^{-2}; and $\alpha = 0.92$ for $p = (1.43, 1.57, 1.75) \times 10^{10}$ cm^{-2}. Inset: $\rho(B_\parallel)$ for $p = 2.26 \times 10^{10}$ cm^{-2}, at different temperatures: $T = 0.1, 0.2, 0.3, 0.45, 0.6, 0.8$ K. (*d*) Magnetoconductivity against $B_\parallel^2$, at $T = 0.6$ K for densities $p = (2.03, 2.26, 2.49, 2.83, 3.36) \times 10^{10}$ cm^{-2}.

rate. Also, according to the previous work on band splitting [23], the magnitudes of the PMR and the rise of ρ with temperature are the same.

In figure 5(*b*) we show a comparative picture of PMR traces at several p in the high-density region. The effect of band splitting seen in the PMR becomes significantly weaker with decreasing density. Thus at $p = 9.4 \times 10^{10}$ cm^{-2} the contribution of the band-splitting effect to the increase of resistivity with increasing temperature cannot exceed 3%. This is negligible in comparison with the experimental resistivity increase of about 50%. At lower p this effect becomes even weaker. This conclusion agrees with the result of [25], where the band splitting is found to be seen only at $p > 1.36 \times 10^{11}$ cm^{-2}.

3.6. Magnetoresistance in the parallel field

Let us now turn to the increase of resistance with parallel field in figure 6(*a*). It was shown recently that the hump in $\rho(B_\parallel)$ corresponds to the magnetic field B_S of full spin polarization of the 2DHG [26]. Our analysis is based on the model [27] of the positive magnetoresistance at $T = 0$, which considers the effect of a parallel field on impurity scattering. Figure 6(*b*) shows $\rho(B_\parallel)/\rho(B_\parallel = 0)$ at the lowest experimental temperature as a function of dimensionless

magnetic field B/B_S, with B_S found as a fitting parameter. (Its value does indeed correspond to the position of the hump, figure 6(a).) Generally, in accordance with [27] all the data collapse onto one curve, which is close to the theoretical dependence, apart from the region near B_S where one can expect a contribution from another mechanism [28]. Using the value of B_S and the fact that m^* is density independent, one can obtain the effective g-factor, $g^* = 2E_F/\mu_B B_S$, whose dependence on the density is shown in the inset to figure 6(b).

The inset to figure 6(c) shows the temperature dependence of the magnetoresistance, where one can see that $B_\parallel$ drives the metallic state into the insulator. To compare this result with the prediction given by equation (2) we analyse the temperature dependence of the resistivity at field B_S. The resulting dependences, figure 6(c), are indeed linear, and by extrapolation to $T = 0$ we find the value of the Drude conductivity σ_0^B, and determine the slope α of the straight lines. Its value is close to the expected $\alpha = 1$, although we find that agreement is better for smaller p, where α increases to 0.92. This can be attributed to the fact that in a real system the scatterers are not exactly point-like, but with decreasing density and increasing Fermi wavelength, $\lambda_F \propto p^{-1/2}$, the approximation of short-range scatterers becomes more applicable.

A detailed analysis of the magnetoresistance at finite temperature can be done at small fields where the discussed interaction theory gives a simple prediction for the magnetoconductivity $\Delta\sigma = \sigma(B_\parallel, T) - \sigma(0, T)$ in the ballistic regime. (We ignore here the contribution of the classical mechanism [27], as the experiment is now performed at significantly higher temperatures, and the Zeeman gap essential for the $T = 0$ model [27] is completely smeared.) The analytical expression [29] for weak fields, $x = \frac{Ez}{2k_BT} \leqslant 1 + F_0^\sigma$ (provided $-0.45 \leqslant F_0^\sigma \leqslant -0.25$), is approximated with 2% accuracy by

$$\Delta\sigma(B_\parallel) = \frac{2F_0^\sigma}{1+F_0^\sigma}\sigma_0\frac{T}{T_F}K_b\left(\frac{Ez}{2T}, F_0^\sigma\right) \tag{6}$$

where $Ez = g_0\mu_B B_\parallel$, g_0 is the bare g-factor (without taking into account the renormalization of the g-factor due to interactions), and $K_b\big(x, F_0^\sigma\big) \approx x^2 f\big(F_0^\sigma\big)/3$, $f(z) = 1 - \frac{z}{1+z}\big[\frac{1}{2} + \frac{1}{1+2z} - \frac{2}{(1+2z)^2} + \frac{2\ln(2(1+z))}{(1+2z)^3}\big]$. In figure 6($b$) we plot the magnetoconductivity at $T = 0.6$ K as a function of $B_\parallel^2$ for fields satisfying the above condition. We use σ_0 obtained in the above analysis at $B_\parallel = 0$. Instead of g_0 we use the value of g^* determined from the analysis of $\rho(B_\parallel)$, at the lowest T. (In doing this, we assume that the experimental value g^* represents the bare g-factor, see section 6.) After that the only unknown parameter in the slope of $\Delta\sigma\big(B_\parallel^2\big)$ is F_0^σ. We extract its value and compare it in figure 3(c) with that determined earlier from $\rho(T)$ at zero field, where a good agreement between the two different approaches is seen.

4. Results on n-Si MOSFETs

The vicinal samples are high-mobility n-Si MOSFETs fabricated on a surface which is tilted from the (100) surface around the [011] direction by an angle of 9.5°. The studied samples have a peak mobility of 2×10^4 cm^2 V^{-1} s^{-1} at $T = 4.2$ K. The electron density has been varied in the range 2×10^{11}–1.4×10^{12} cm^{-2}.

The temperature dependence of the resistivity has been measured in a wide temperature range (see figure 7(a)) . It is seen that the dependence changes with decreasing n from metallic to insulating, although, in general, $\rho(T)$ has a complicated non-monotonic character. The low-temperature results were analysed in detail in [30]. Here we concentrate only on the metallic behaviour seen at larger densities at $T > 4$ K and before the transition to the nondegenerate state at $T \sim T_F$ (marked by a dashed line in figure 7(a)). The phonon scattering can be neglected in this regime as in Si structures it only becomes important at $T > 100$ K [5].

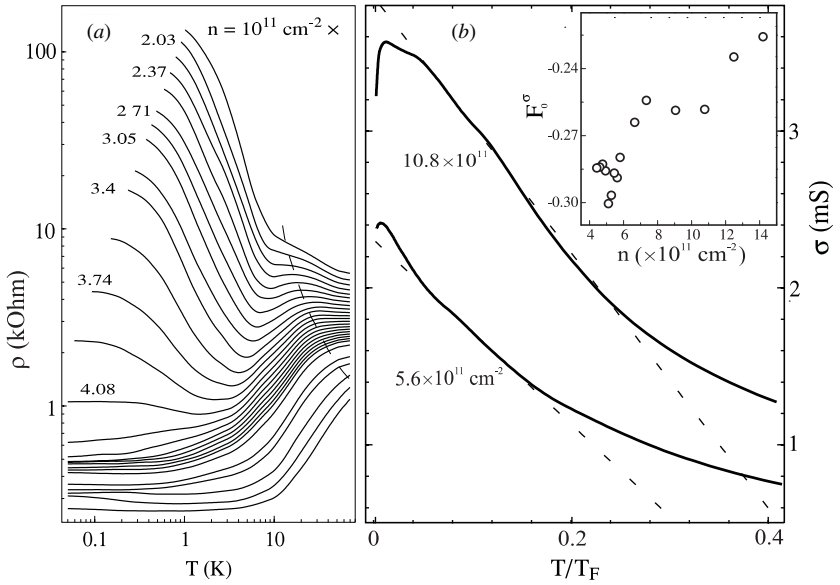

Figure 7. (*a*) Temperature dependence of resistivity at different densities for the 2DEG in the vicinal Si MOSFET. Electron concentration is changed from $n = 1.85 \times 10^{11}$ cm^{-2} to $n = 12.5 \times 10^{11}$ cm^{-2} (bottom curve). Dashed line marks the Fermi temperature T_F. (*b*) An example of a linear fit of the same data in the conductivity form, for two densities. The inset shows the parameter F_0^σ as a function of the electron density.

Figure 7(*b*) shows an example of the temperature dependence in the conductivity form. We fit the linear part of $\sigma(T)$ by the theory of interactions in the ballistic regime, using the relation $\delta\sigma(T) = \sigma_0\big(1 + \frac{15F_0^\sigma}{1+F_0^\sigma}\big)\frac{k_B T}{2E_F}$, relevant to 2DEGs in Si with double valley degeneracy [31]. This situation is realized at weak intervalley scattering and for a small intervalley gap. We have performed the analysis of the linear $\rho(T)$ assuming that this is the case. The obtained parameter F_0^σ increases with decreasing density, figure 7(*b*) (inset), in agreement with previous results (figure 3(*c*)). Strong intervalley mixing would reduce the linear T-dependence to equation (1), which we also used to determine F_0^σ presented in figure 8(*d*) and discussed later.

5. Results on n-GaAs

To examine the prediction of interaction theory for a long-range scattering potential [9] we have used a 2DEG in a standard modulation doped n-GaAs heterostructure with a thin spacer $d = 200$ Å. The mobility changes in the range $(0.42\text{–}5.5) \times 10^5$ cm^2 V^{-1} s^{-1} when the electron density is increased from 0.46×10^{11} to 2×10^{11} cm^{-2}. This allows us to vary the parameter $k_B T\tau/\hbar$ in a broad range from 0.04 to 3.8 in the studied temperature interval $T = 0.2\text{–}1.2$ K.

In this structure we observe parabolic negative magnetoresistance (NMR), shown in figures 8(*a*) and (*b*) for the density $n = 6.8 \times 10^{10}$ cm^{-2}, in agreement with the prediction of interaction theory [9] for a long-range random potential (equation (3), section 2). The $k_F d$ value varies from 1.2 to 2.2 which proves that the fluctuation potential with the correlation length d (spacer width) is indeed long range. This is further supported by the fact that the momentum relaxation time in these structures is much larger than the quantum lifetime

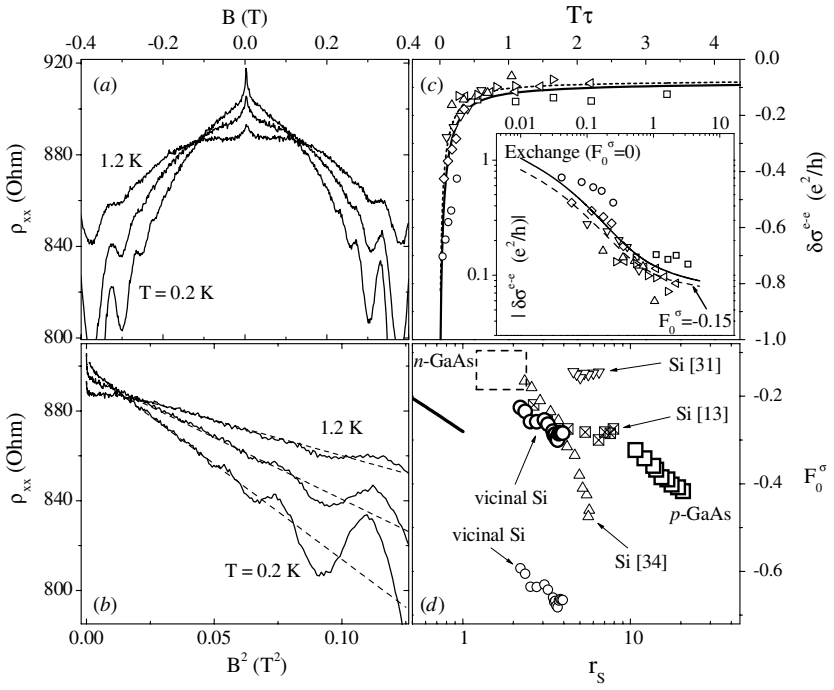

Figure 8. Longitudinal resistivity versus magnetic field for electron density $n = 6.8 \times 10^{10}$ cm^{-2} at different temperatures: $T = 0.2$, 0.8, 1.2 K. (*b*) The same data presented as a function of B^2. (*c*) Interaction correction obtained for different electron densities, $n = (0.46\text{–}2.0) \times 10^{11}$ cm^{-2} (different symbols). Solid line: theoretical prediction [9] for the correction due to the exchange interaction, shifted by $-0.07e^2/h$. Dashed line: theory for the total correction with $F_0^\sigma = -0.15$. Inset: the same results presented in the logarithmic scales. (*d*) The dependence of the Fermi liquid parameter on r_s for different systems. The values of F_0^σ for the 2DEG in the vicinal Si structures have been found using the two-valley approach (large circles) and one-valley approach, equation (1), (small circles). The dashed box encloses the estimated values for the 2DEG in n-type GaAs heterostructure. Solid line is the theoretical curve for small r_s [4].

($\tau \gg \tau_q$). The magnetoresistance is analysed in the range $\omega_c\tau > 1$ to satisfy the condition of the theory [9].

In figure 8(*a*) the NMR exhibits a sharp change in small fields caused by weak localization, followed by a parabolic dependence. We analyse the parabolic NMR in the range of fields well above the 'transport' magnetic field $B_{\rm tr} = \hbar/4De\tau \sim 0.013$ T in order to suppress weak localization. (We have also confirmed [32] that the magnetic field is not large enough for the development of the magnetoresistance caused by the Zeeman effect on the interaction correction [2].)

In figure 8(*b*) the resistivity is plotted as a function of B^2 and from the slope of the straight line $\delta\sigma_{xx}^{ee}(T)$ is obtained. Figure 8(*c*) shows the temperature dependence of $\delta\sigma_{xx}^{ee}$ for different electron densities, where experimental points concentrate around one curve. This curve becomes close to the interaction correction in the exchange channel [9] if one makes a vertical shift of the theoretical dependence by $\Delta\sigma = -0.07e^2/h$ (there are no other adjustable parameters). We believe [32] that the physical origin of this additional, temperature-independent contribution is the classical quadratic NMR [33].

It is important to emphasize that the comparison was made with the contribution from the exchange channel only, however it is known that there is another (Hartree) term in interactions

controlled by the parameter F_0^σ. Comparing the total correction (exchange plus Hartree [9]) with the experiment shows that the Hartree contribution is much smaller than the exchange contribution. It can be seen in figure 8(*c*) (inset) that within experimental error the magnitude of the parameter F_0^σ in our case cannot be larger than 0.1–0.2.

In figure 8(*d*) we plot the values of F_0^σ obtained from experiments on the 2DHG in GaAs (figure 3(*c*)) and the 2DEG in vicinal Si (figure 7(*b*), inset), as well as the recent results on the 2DEG in (100) Si MOSFETs [13, 31, 34]. All these values were obtained on systems with point-like scattering using the theory [4]. On the same plot we indicate a possible range of F_0^σ in our 2DEG in GaAs with long-range potential, as the experimental accuracy does not allow us to establish the density dependence of F_0^σ. The overall trend of $F_0^\sigma(r_s)$ from large to small r_s in figure 8(*d*) shows that our estimation of F_0^σ in our case is reasonable, and consistent with other results.

6. Discussion

The comparison of the interaction parameters F_0^σ in figure 8(*d*) contains an assumption that the character of carrier–carrier scattering is the same in different structures. It also has to be noted that the results of analysis for 2DEG in Si depend strongly on the intensity of intervalley scattering and the relation between the valley splitting Δ and temperature. In [13] it was assumed that $\Delta > k_B T$, while in [31, 34] the opposite assumption is made. The difference in the assumptions can be reflected in the determined value of F_0^σ, as different expressions are taken in the Hartree term of the temperature dependence. If we use equation (1) for the analysis of Si data (assuming strong intervalley scattering or very large Δ), the value of $\left|F_0^\sigma\right|$ will be significantly larger in magnitude and out of the general trend in figure 8(*d*).

It is seen in figure 6(*b*) (inset) that the g-factor of holes in GaAs strongly decreases with decreasing density—a similar behaviour was recently observed for 2D electrons [17] and holes [35] in GaAs. This does not agree with the expectation of the interaction theory, where the renormalization of the bare g-factor should lead to an increase of g^* (such an increase was seen in the 2DEG in Si [12, 36]). Therefore, we assumed in section 3.6 that the observed $g^*(n)$ represents the bare g-factor. Recently, it was suggested in [37] that for 2DEG in GaAs such $g(n)$-dependence can be caused by the effect of the parallel field on the effective mass, due to the finite thickness of the electron channel. In the case of holes such behaviour of the g-factor requires further investigation. The observed decrease of the g-factor can be attributed to the complex band structure of holes in GaAs. It is expected that in a 2D hole system the bare g-factor measured in parallel magnetic field is close to zero when $k_\parallel$ approaches the zero value. This can explain the tendency of the effective g-factor of holes to decrease with lowering p.

It is interesting to note that in figure 3(*b*) one can see saturation in $\sigma(T)$ at low temperatures. Similarly, in figure 7(*b*) there is a change in the sign of $\mathrm{d}\sigma/\mathrm{d}T$ at low T. This behaviour of the conductivity is in qualitative agreement with theory [4] where the change of the sign of $\mathrm{d}\sigma/\mathrm{d}T$ is expected with decreasing temperature, at the transition from the ballistic regime to the diffusive regime. We find, however, that in the experiment the deviation from the linear dependence $\sigma(T)$ occurs at higher temperatures than expected (e.g., in figure 3(*b*) it is seen at $k_B T\tau/\hbar \sim 1$ instead of the expected $k_B T\tau/\hbar \sim 0.1$). We think that the reason for this change in $\sigma(T)$ is additional contributions appearing at lower temperatures. In the 2DHG it is probably due to the effect of weak localization. In the case of the 2DEG on vicinal Si the deviation is caused by the complicated low-temperature behaviour of the conductance described in [30].

In our experiments the character of the scattering potential in the two studied GaAs/AlGaAs structures is different: it is short range in the 2DHG and long range in the 2DEG. If only one type of scatterers was present, one would expect that $\tau \sim \tau_q$ for short-range scatterers and $\tau \gg \tau_q$ for long-range scatterers. In reality both types are present, so that the condition $\tau > \tau_q$ is seen in both structures. This is a clear signature of the presence of a long-range potential. In the 2DHG it is weaker because of the larger spacer in the structure, so that the effect of short-range scattering produced by background impurities becomes visible (figure 4). Short-range scatterers make a significant contribution to τ, as a long-range potential does not produce the required large-angle scattering. Thus, in the case of mixed scatterers in the 2DHG the domination in τ of short-range potential is accompanied by the condition $\tau > \tau_q$ rather than $\tau \sim \tau_q$ expected for purely short-range scatterers.

7. Conclusion

We have demonstrated that in a GaAs heterostructure with a short-range random potential the metallic character of $\rho(T)$ near the metal-to-insulator transition and the positive magnetoresistance in parallel field are caused by the hole–hole interaction in the ballistic limit $k_B T\tau/\hbar > 1$. We have found the Fermi liquid constant $F_0^\sigma(p)$, which determines the sign of $\rho(T)$. In zero magnetic field, the value of the interaction constant was obtained from the metallic $\rho(T)$ of a 2DEG in vicinal Si MOSFETs, where scattering is also determined by a short-range impurity potential.

The predictions of the interaction theory beyond the short-range approximation were tested in a 2DEG in a GaAs heterostructure, where the electron scattering is determined by a long-range fluctuation potential. We have observed a parabolic negative magnetoresistance in strong magnetic field and used it to find the electron–electron interaction correction in the intermediate and ballistic regimes.

Acknowledgments

We are grateful to I L Aleiner, B L Altshuler, B N Narozhny, I V Gornyi and A D Mirlin for stimulating discussions and valuable comments, and EPSRC and ORS award funds for financial support.

References

[1] Abrahams E, Kravchenko S V and Sarachik M P 2001 *Rev. Mod. Phys.* **73** 251
[2] Altshuler B L and Aronov A G 1985 *Electron-Electron Interaction in Disordered Systems*ed A L Efros and M Pollak (Amsterdam: North-Holland)
[3] Finkelstein A M 1983 *Sov. Phys.–JETP* **57** 97
[4] Zala G, Narozhny B N and Aleiner I L 2001 *Phys. Rev.* B **64** 214204
[5] Ando T, Fowler A and Stern F 1982 *Rev. Mod. Phys.* **54** 437
[6] Shayegan M *et al* 1988 *Appl. Phys. Lett.* **52** 1086
Shayegan M *et al* 1988 *Appl. Phys. Lett.* **53** 2080
[7] Gold A 1990 *Phys. Rev.* B **41** 8537
Gold A 1991 *Phys. Rev.* B **44** 8818
[8] Hirakawa K *et al* 1986 *Phys. Rev.* B **33** 8291
[9] Gornyi I V and Mirlin A D 2002 *Preprint* cond-mat/0207557
[10] Proskuryakov Y Y *et al* 2001 *Phys. Rev. Lett.* **86** 4895
[11] Chen G-H and Raikh M E 1999 *Phys. Rev.* B **59** 5090
[12] Pudalov V M *et al* 2002 *Phys. Rev. Lett.* **88** 196404
[13] Shashkin A A *et al* 2002 *Phys. Rev.* B **66** 073303

[14] Isihara A and Smrǒka L 1986 *J. Phys. C: Solid State Phys.* **19** 6777
[15] Coleridge P T *et al* 1989 *Phys. Rev.* B **39** 1120
[16] Hirakawa K *et al* 1993 *Phys. Rev.* B **47** 4076
Stormer H L *et al* 1983 *Phys. Rev. Lett.* **51** 126
[17] Tutuc E *et al* 2002 *Phys. Rev. Lett.* **88** 036805
[18] Karpus V 1990 *Semicond. Sci. Technol.* **5** 691
[19] Das Sarma S and Hwang E H 2000 *Phys. Rev.* B **61** R7838
[20] Mills A P *et al* 1999 *Phys. Rev. Lett.* **83** 2805
[21] Van Hall P J 1989 *Superlattices Microstruct.* **6** 213
[22] Proskuryakov Y Y *et al* 2002 *Phys. Rev. Lett.* **89** 076406
[23] Murzin S S and Dorozhkin S I 1998 *JETP Lett.* **67** 113
[24] Yaish Y *et al* 2000 *Phys. Rev. Lett.* **84** 4954
[25] Yaish Y *et al* 2001 *Preprint* cond-mat/0109469
[26] Tutuc E *et al* 2001 *Phys. Rev. Lett.* **86** 2858
[27] Dolgopolov V T and Gold A 2000 *JETP Lett.* **71** 27
[28] Das Sarma S *et al* 2000 *Phys. Rev. Lett.* **84** 5596
[29] Zala G *et al* 2001 *Phys. Rev.* B **65** 020201
[30] Safonov S S *et al* 2001 *Phys. Rev. Lett.* **86** 272
[31] Vitkalov S A *et al* 2002 *Preprint* cond-mat/0204566
[32] Li L *et al* 2003 *Phys. Rev. Lett.* **90** 076802
[33] Mirlin A D *et al* 2001 *Phys. Rev. Lett.* **87** 126805
[34] Pudalov V M *et al* 2002 *Preprint* cond-mat/0205449
[35] Noh H *et al* 2002 *Preprint* cond-mat/0206519
[36] Shashkin A A *et al* 2001 *Phys. Rev. Lett.* **87** 086801
[37] Tutuc E *et al* 2003 *Preprint* cond-mat/0301027